Supporting Information

Rutten *et al.* 10.1073/pnas.0813064106

SI Text

Results. ***Phasing and multicrystal and noncrystallographic symmetry (NCS) averaging.*** After the location of seven Zn^{2+} sites (one of the zinc ions is located on either a crystallographic or a noncrystallographic symmetry axis in $P2_12_12$ and P2, respectively) phases were calculated with ShelxD, and density modification was performed by using a solvent content of 55%, taking into account the presence of two molecules in the asymmetric unit. The final solvent plus detergent content is 61.5%, and the V_m is 3.2 (the same for both the $P2_12_12$ and P2 space groups). Unfortunately, both electron density maps turned out to be of very poor quality; electron density was very discontinuous and thus not interpretable. This is possibly because of the low quality of the diffraction data of the P2 crystal and the low anomalous dispersion of zinc in the $P2_12_12$ data. By using only data up to 4-Å resolution of the P2 dataset, a more continuous electron density map was obtained, suggesting a 12-stranded β-barrel fold. Density for side chains and for large parts of some strands was lacking. The C-terminal transporter part of the NalP autotransporter, of which the crystal structure had been solved before (1), was used to make a backbone model with ≈80% of the amino acid residues. This very incomplete model was used to generate a mask around the protein molecule and was used to perform Molecular replacement (MR) with the program PHASER (2). From the correct MR solutions for the two datasets, we generated accurate rotation/translation matrices from one molecule in the P2 space group to the NCS-related molecule and to the two molecules in the asymmetric unit of the $P2_12_12$ space group. In the $P2_12_12$ crystal packing, an NCS dimer is formed with both molecules at the same height along the *c* axis. In crystals belonging to the P2 space group, a crystallographic 2-fold symmetry axis is present between these molecules. In these crystals, the NCS axis is almost parallel to the diagonal between the *a* and *c* axis, which coincides approximately with the *a* axis in $P2_12_12$. The P2 space group can be transformed to a cell that is twice as large, with cell dimensions of $a = 109.4$ Å, $b = 128.4$ Å, $c = 60.97$ Å, and $\beta = 93.8°$, which is approximately the same as in $P2_12_12$ space group. Phases from ShelxE, the rotation/translation matrices, and the mask were used to perform multicrystal and noncrystallographic averaging with the program DMMULTI in the CCP4 suite (3), yielding a high-quality electron density map, allowing tracing of the whole protein.

Zinc sites in LpxR. The LpxR structure contains two LpxR molecules and nine Zn^{2+} ions in the asymmetric unit. The two LpxR molecules in the asymmetric unit are oriented toward each other as shown in Fig. S2. The program PISA of the EMBL-EBI calculated a complexation significance score of only 0.037, which implies that the interface is not significant for complexation and that it may be solely a result of crystal packing. The surface interface area between the two LpxR molecules in A.S.U. is 707.4 Å^2. The total area of one LpxR molecule is 12,816.4 Å^2, which makes the interface area only 5.5% of the total area. Size-exclusion chromatography with a Superdex 200 10/300 GL column showed that LpxR (32 kDa) eluted at 14.3 mL and that BSA (66 kDa), which was chosen as a control, eluted at 14.8 mL. The micelle mass was subtracted from the estimated elution mass of LpxR. Based on a micelle mass for DDM, which is between 39.8 and 76 kDa, a monomeric state for LpxR in solution is most likely.

In the interface between both LpxR molecules in the asymmetric unit, there are four Zn^{2+} ions coordinated at the periplasmic side (Fig. S2). These four zinc ions (Zn1, Zn2, and Zn_ncs1 and Zn_ncs2) are very close together and liganded by S42, H43, Y41, and D44. Furthermore, there are some hydrophilic interactions at the extracellular side of the molecules. In the helix of L3, R123 makes a salt bridge with D111 of the NCS-related molecule and vice versa. R120 forms a hydrogen bond with the backbone oxygen of D134, and vice versa. One zinc (Zn3) in each of the NCS molecules is present inside the β-barrel, indicating that zinc can enter the solution-filled cavity inside the barrel. It is liganded by H54, H84, and D104. The fourth zinc (Zn4) that was found by ShelxD is present on a special position and is coordinated by ND1 of H25 and OD2 of D29, and the same residues form a symmetry-related molecule. Zn5 was not found with ShelxD but only after refinement and subsequent calculation of the anomalous difference electron density map.

Materials and Methods. ***Sequence alignment of LpxR homologs.*** Sequences of LpxR homologs were aligned by using ClustalX (4). The alignment was optimized by removing gaps that aligned within the membrane-embedded regions of LpxR of *Salmonella typhimurium*.

Production of LpxR in inclusion bodies. To produce LpxR in cytoplasmic inclusion bodies, the predicted coding region for LpxR minus the signal sequence was amplified by PCR from *S. typhimurium* strain LT2 genomic DNA by using the oligonucleotides LpxR(−)FW and LpxR(−)REV (Table S4). The PCR product was subcloned into the NdeI and BamHI restriction sites of pET21a (Novagen), and the resulting plasmid was designated pLpxR(−). For production of the protein we used *Escherichia coli* BL21Star(DE3) (Novagen). A colony of BL21Star(DE3)/pLpxR(−) was inoculated in 1 mL of LB broth containing 0.2% glucose (wt/vol) and 100 μg of ampicillin. After 6 h of growth at 37 °C, the culture was used to inoculate 1 L of prewarmed autoinduction LB broth medium containing 50 mM phosphate buffer (pH 6.9), 5 mM Mg_2Cl, 0.5% glycerol (vol/vol), 0.2% glucose (wt/vol), 0.002% lactose (wt/vol), and 100 μg/mL ampicillin. Cells were grown for 18 h at 240 rpm and 37 °C.

LpxR assays. LpxR activity was measured as described in ref. 5 in a 20-μL reaction mixture containing 50 mM Mes (pH 6.5), 1.0% Triton X-100, 5 mM $CaCl_2$, and 2.5 μM Kdo_2–[4′-^{32}P]lipid A (≈10,000 cpm/nmol) as the substrate. ^{32}P-labeled lipid substrates were prepared as described in ref. 6. For routine assays, reactions were carried out at 30 °C by using either washed membranes or purified protein as the enzyme source at the indicated protein concentrations. Assays were terminated by spotting 4.5-μL portions of the mixtures onto silica gel 60 TLC plates. Reaction products were separated by using the solvent chloroform, pyridine, 88% formic acid, water (30:70:16:10, vol/vol), and visualized by PhosphorImaging analysis. To demonstrate that imidazole restored activity of the H122A mutant, membranes (0.001 mg/mL) containing LpxR H122A were assayed as described above for deacylase activity in the presence of increasing concentrations of imidazole (25, 50, and 100 mM). To determine whether LpxR activity was inhibited by the chemical modifier diethylpyrocarbonate, pure LpxR (1 μM) was exposed to either 0.1 or 1 mM concentrations of diethylpyrocarbonate for 10 min. Reactions containing diethylpyrocarbonate were quenched by using 10-fold excess imidazole. The chemically modified LpxR was then assayed for deacylase activity as described above at a final protein concentration of 5×10^{-5} mg/mL.

1. Oomen CJ, *et al.* (2004) Structure of the translocator domain of a bacterial autotransporter. *EMBO J* 23:1257–1266.
2. McCoy AJ, Grosse-Kunstleve RW, Storoni LC, Read RJ (2005) Likelihood-enhanced fast translation functions. *Acta Crystallogr D* 61:458–464.
3. Cowtan K (1994) ''dm'': An automated procedure for phase improvement by density modification. *Joint CCP4 and ESF-EACBM Newsletter on Protein Crystallography* 31:34–38.
4. Chenna R, *et al.* (2003) Multiple sequence alignment with the Clustal series of programs. *Nucleic Acids Res* 31:3497–3500.
5. Reynolds CM, *et al.* (2006) An outer membrane enzyme encoded by *Salmonella typhimurium lpxR* that removes the 3′-acyloxyacyl moiety of lipid A. *J Biol Chem* 281:21974–21987.
6. Tran AX, *et al.* (2004) Periplasmic cleavage and modification of the 1-phosphate group of *Helicobacter pylori* lipid A. *J Biol Chem* 279:55780–55791.
7. Raetz CR, Reynolds CM, Trent MS, Bishop RE (2007) Lipid A modification systems in Gram-negative bacteria. *Annu Rev Biochem* 76:295–329.
8. Raetz CR, Whitfield C (2002) Lipopolysaccharide endotoxins. *Annu Rev Biochem* 71:635–700.
9. Touze T, Tran AX, Hankins JV, Mengin-Lecreulx D, Trent MS (2008) Periplasmic phosphorylation of lipid A is linked to the synthesis of undecaprenyl phosphate. *Mol Microbiol* 67:264–277.
10. Trent MS, Stead CM, Tran AX, Hankins JV (2006) Diversity of endotoxin and its impact on pathogenesis. *J Endotoxin Res* 12:205–223.
11. Jorgensen WL, Tirado-Rives J (1988) The OPLS (optimized potentials for liquid simulations) potential functions for proteins, energy minimizations for crystals of cyclic peptides, and crambin. *J Am Chem Soc* 110:1657–1666.
12. Fernandez-Recio J, Totrov M, Abagyan R (2004) Identification of protein–protein interaction sites from docking energy landscapes. *J Mol Biol* 335:843–865.

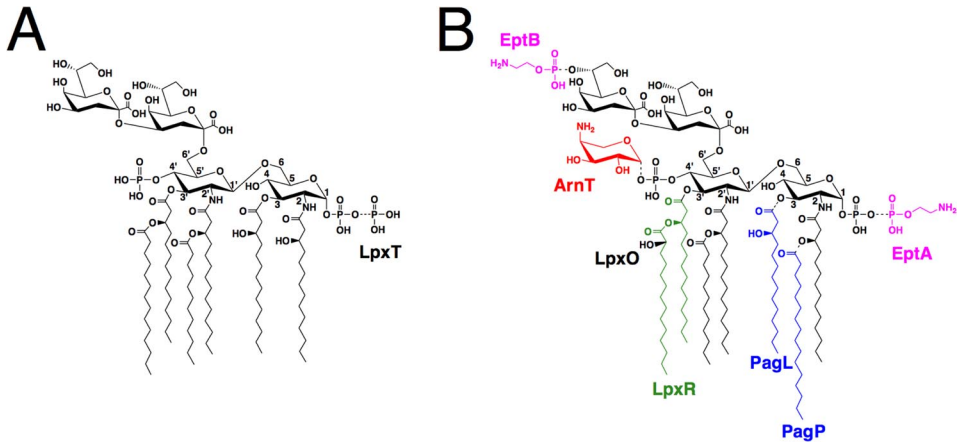

Fig. S1. Comparison of *S. typhimurium* Kdo_2–lipid A and its modified forms. (*A*) The synthesis of unmodified *bis*-phosphorylated Kdo_2–lipid A of *S. typhimurium* requires nine enzymatic steps (7, 8). An additional phosphate group can be attached at the 1 position catalyzed by LpxT (9). (*B*) Activation of the transcriptional regulators PhoP and PmrA during exposure to various environmental stimuli leads to modification of the lipid A structure (7, 8). The phosphate groups can be replaced with 4-amino-4-deoxy-L-arabinose (red) by the L-4-aminoarabinose transferase (ArnT) and/or phosphoethanolamine (magenta) by the phosphoethanolamine transferase (EptA) (7, 10). An additional phosphoethanolamine group (magenta) can be added to the outer Kdo sugar by the enzyme EptB. LpxO, an oxygen-dependent hydroxylase, is required for the hydroxylation of the secondary fatty acyl chain at the 3′ position (black) (7, 8). The outer membrane enzymes PagP and PagL catalyze the addition of the secondary palmitate at the 2 position (blue) or the removal of the ester-linked *R*-3-hydroxymyristate group at the 3 position (blue), respectively (7, 8). LpxR removes the 3′-*O*-linked acyloxyacyl group (green) in a Ca^{2+}-dependent manner (5).

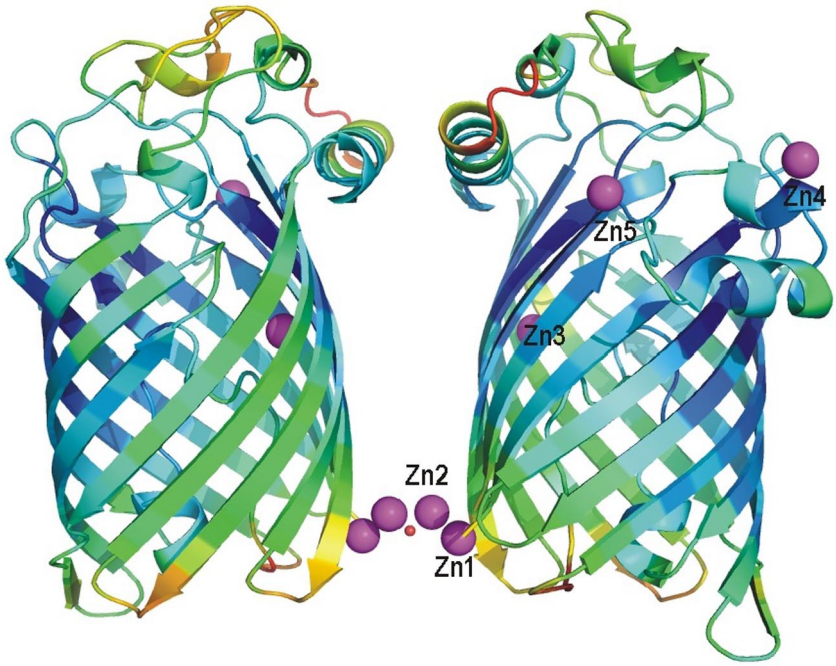

Fig. S2. Representation of the NCS dimer of LpxR in the $P2_12_12$ space group. The ribbon is colored with colors representing the temperature factor of the C^{α} atoms. Atoms with low-temperature factors are colored blue, and the atoms with high-temperature factors are colored red. Zn^{2+} ions are shown as magenta spheres, and a water molecule as a small red sphere. Zinc ions are labeled in one of the NCS molecules. The figure was created with PyMOL.

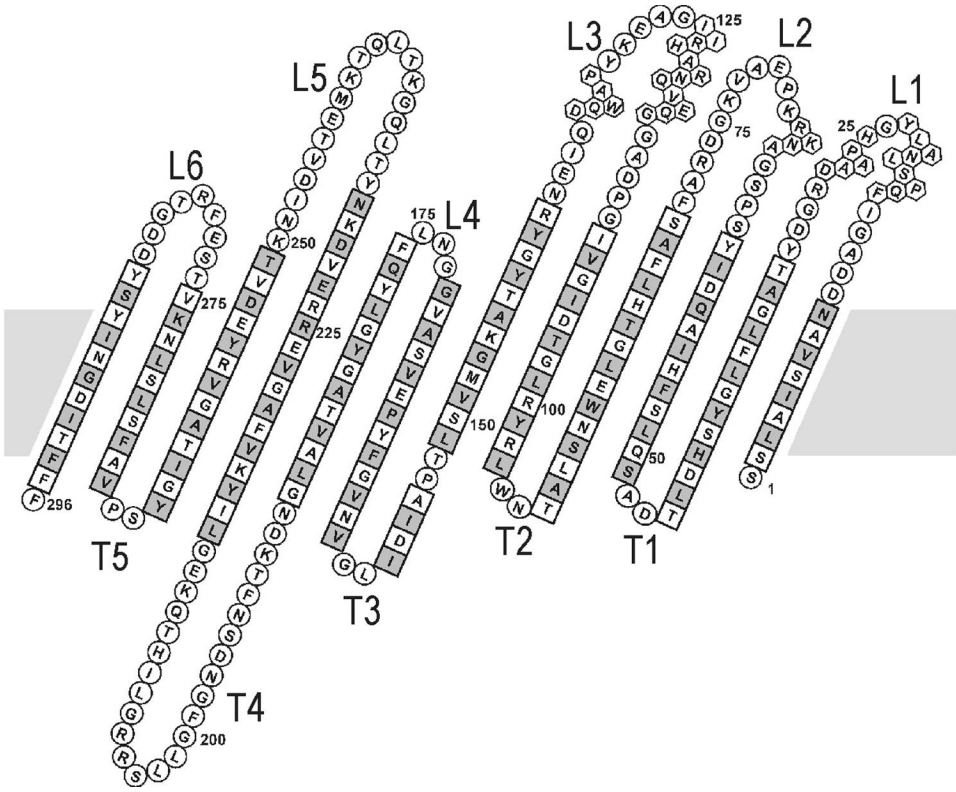

Fig. S3. Topology model of LpxR. Amino acid residues are given in one-letter code. Squares represent residues that are present in the β-strands. Side chains of amino acids that are shaded gray point to the outside of the barrel. Amino acids in the α-helical regions are represented as hexagons.

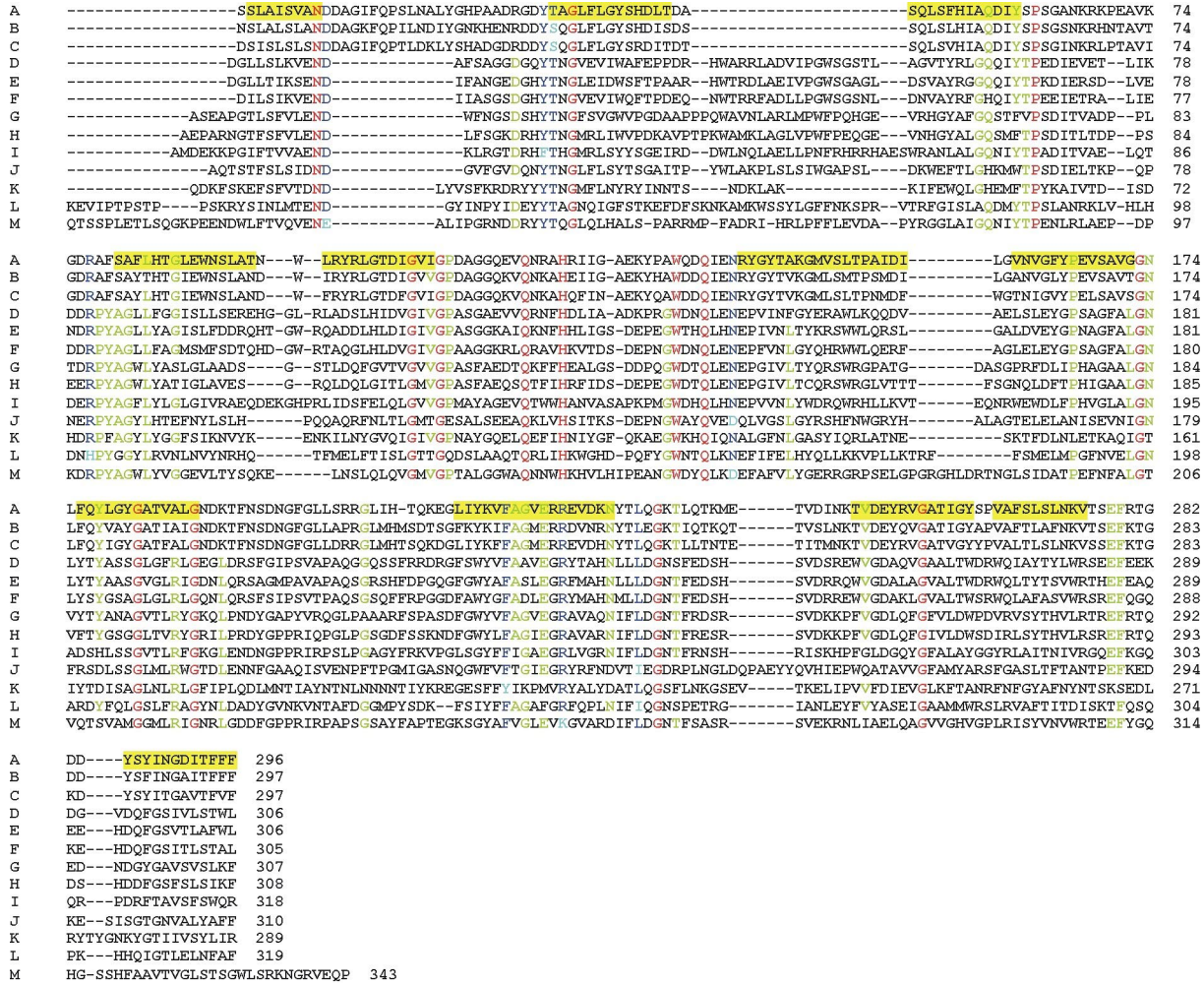

Fig. S4. Sequence alignment of LpxR homologs. (*A*) *S. typhimurium* (NP_460294). (*B*) *E. coli* O157:H7 strain Sakai (NP_308841). (*C*) *Yersinia enterocolitica* 8081 (CAL13076). (*D*) *Marinobacter aquaeoli* VT8 (YP_957868). (*E*) *Chromohalobacter salexigens* (ABE58654). (*F*) *Pseudomonas stutzeri* A1501 (YP_001172025). (*G*) *Thiobacillus denitrificans* (AAZ97232). (*H*) *Synthrophus aciditrophicus* SB (ABC79036). (*I*) *Delta proteobacterium* MLMS-1 (EAT02306). (*J*) *Vibrio cholerae* O1 eltor (NP_231501). (*K*) *Tenacibaculum* sp. MED152 (ZP_01051679). (*L*) *Helicobacter pylori* (NP_223352). (*M*) *Caulobacter* sp. K31 (EAU12240). β-Strands in the solved LpxR structure are represented as a yellow background; residues that are fully conserved in all aligned sequences are colored red; highly conserved residues are colored in blue; residues with only few conservative substitutions are shown in turquoise in few of the aligned sequences; other highly conserved residues, present in at least 9 of the 13 aligned sequences, are shown in olive. All sequences are shown without the putative signal sequences.

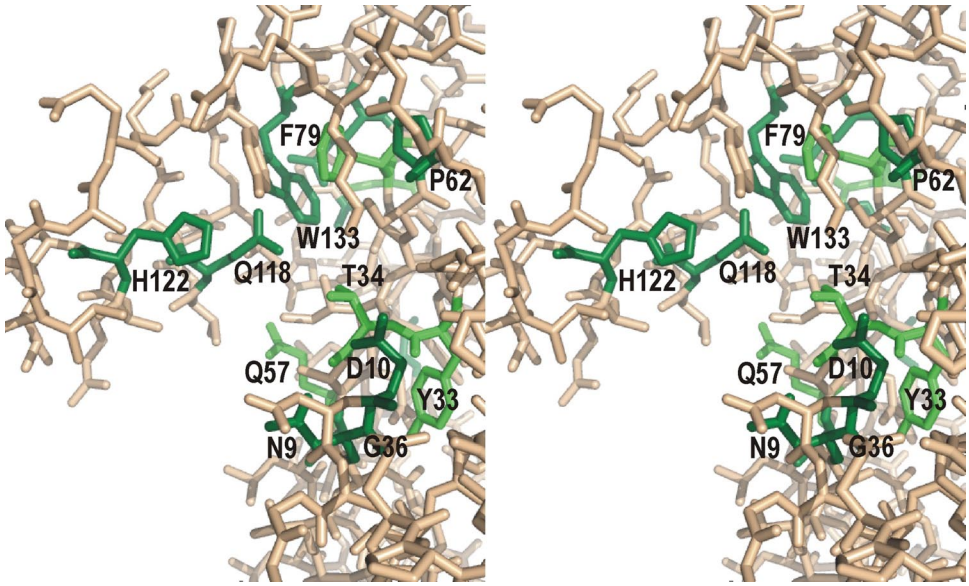

Fig. S5. Stereo representation of a closeup of the active site of LpxR. Nonconserved residues are in wheat color. Fully conserved residues are shown in dark green, and residues that are largely conserved are shown in light green. Conserved residues directing toward the active-site cleft are labeled. The figure was created with PyMOL.

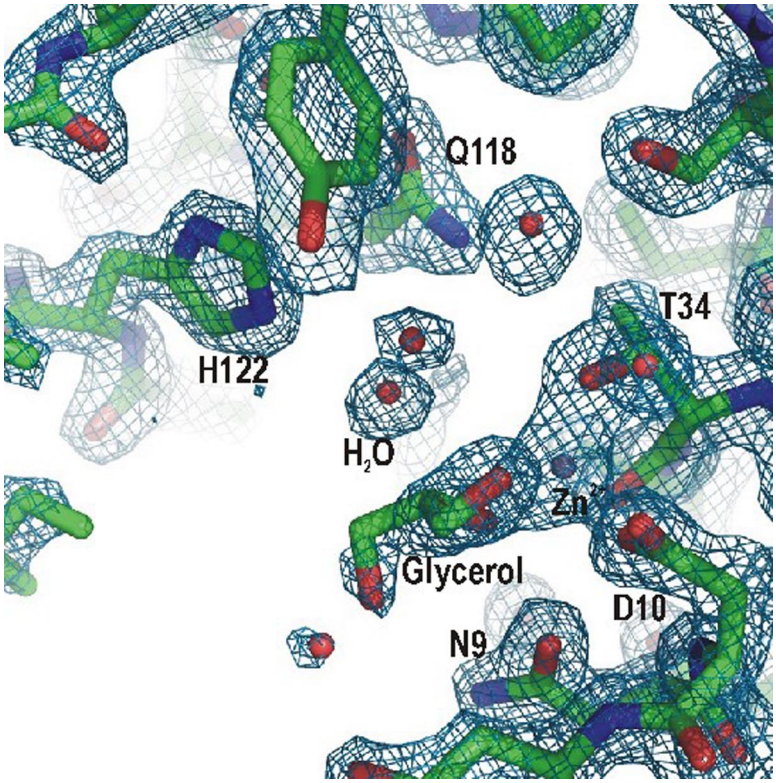

Fig. S6. Electron density in the active site. Part of the LpxR structure is shown as sticks. Water molecules are represented as small red spheres. $2F_o - F_c$ electron density is shown at 1.2σ as blue chicken wire.

Table S1. 3′-*O*-deacylase activities of mutant LpxR proteins

Mutation	Relative activity, % wild type*
N9A	NoActivity
D10A	NoActivity
T34A	No activity
T34S	62
S61A	77
S63A	95
Q118A	6
H122A	No activity
H122Q	No activity

Standard LpxR assays were performed with whole membranes from *E. coli* W3110 expressing either wild-type or mutant LpxRs. Assays were carried out in the linear range of assay using Kdo_2–lipid A as substrate. The level of activity shown is relative to that of wild-type LpxR under identical assay conditions in the presence of 5 mM Ca^{2+}.

Table S2. Statistics of HADDOCK results for the various clusters

Cluster	HADDOCK score, a.u.*	Ligand rmsd, Å†	Ligand rmsd E_{min}, Å‡	No. of structures in cluster	E_{vdw}§, kcal mol^{-1}	E_{elec}¶, kcal mol^{-1}	E_{desol}, kcal mol^{-1}	Buried surface area, Å^2
1	−139 ± 8	3.6 ± 1.4	3.6 ± 1.4	152	−39 ± 5	−494 ± 24	9.6 ± 5.6	1,665 ± 112
2	−128 ± 4	3.6 ± 1.3	4.7 ± 1.1	16	−36 ± 7	−447 ± 38	7.6 ± 6.4	1,582 ± 138
5	−106 ± 10	3.4 ± 1.7	5.0 ± 1.0	6	−32 ± 5	−411 ± 61	16.3 ± 7.1	1,375 ± 193
3	−104 ± 8	4.7 ± 1.6	7.0 ± 0.7	12	−29 ± 8	−421 ± 36	19.2 ± 5.0	1,318 ± 124
4	−93 ± 8	3.3 ± 1.5	15.1 ± 0.4	7	−40 ± 6	−366 ± 34	24.4 ± 7.0	1,448 ± 90

Average ± SD were calculated over the top four structures of each cluster. Clustering was performed with a 3.5-Å cutoff based on the ligand rmsd matrix.

*The HADDOCK score in arbitrary units (a.u.) calculated as:

HADDOCK score = 1.0 * E_{vdw} + 0.2 * E_{elec} + 0.1 * E_{AIR} + 1.0 * E_{deso}. E_{vdw} represents the Van der Waals energy, E_{elec} represents the electrostatic energy, E_{AIR} represents the energy from the ambiguous interaction restraints, and E_{deso} represents the empirical desolvation energy term.

†Average rmsd and SD from the lowest energy structure of the cluster. Structures were superimposed on the backbone atoms of LpxR, and the rmsd values were calculated on the heavy atoms of Kdo_2–lipid A excluding the lipid tails.

‡Average rmsd and SD from the overall lowest energy. Structures were superimposed on the backbone atoms of LpxR, and the rmsd values were calculated on the heavy atoms of Kdo_2–lipid A excluding the lipid tails.

§The nonbonded energies were calculated with the OPLS parameters (11) using a 8.5-Å cutoff.

¶Empirical desolvation energy (12).

Table S3. Data collection and refinement statistics

Parameters	Dataset 1	Dataset 2
Data collection		
Space group	$P2_12_12$	P2
Cell dimensions, Å		
a	106.9	81.1
b	127.7	60.5
c	60.7	86.6
β, °		99.1
Resolution, Å (outer shell)	1.9 (2.00)	2.3 (2.42)
R_{sym}	0.159 (0.805)	0.124 (0.595)
$R_{pim\ (all\ I+\ and\ I-)}$	0.044 (0.220)	0.093 (0.412)
I/σ, I	14.7 (3.6)	11 (2.2)
Completeness, %	100 (100)	87.4 (93.3)
Redundancy	14.9 (15.0)	3.5 (3.6)
Refinement		
Resolution, Å	1.9	
No. reflections	62,825	
R_{work}/R_{free}	0.191/0.230	
No. atoms	5,183	
Protein	2	
Ligand/ion	8 $C_{10}E_5$ parts, 4 glycerol/9 Zn^{2+}	
Water	414	
Mean *B* value, Å^2	17.7	
rmsd		
Bond lengths, Å	0.014	
Bond angles, °	1.54	

Table S4. Oligonucleotides

Name*	Sequence†
LpxR(−) FW	5′-GCGCGCCATATGAGTAGCCTTGCTATTTCAGTG-3′
LpxR(−) REV	5′-GCGCGCGGATCCTCAGAAGAAGAAGGTGATGTCTCC-3′
N9A FW	5′-GTAGCCTTGCTATTTCAGTGGCGGCGGATGATGCAGGTATATTTCAACC-3′
N9A REV	5′-GGTTGAAATATACCTGCATCATCCGCCGCCACTGAAATAGCAAGGCTAC-3′
D10A FW	5′-CTTGCTATTTCAGTGGCGAATGCCGATGCAGGTATATTTCAACC-3′
D10A REV	5′-GGTTGAAATATACCTGCATCGGCATTCGCCACTGAAATAGCAAG-3′
T34A FW	5′-TGCAGACCGGGGTGATTATGCGGCCGGGCTCT-3′
T34A REV	5′-AGAGCCCGGCCGCATAATCACCCCGGTCTGCA-3′
T34S FW	5′-GCAGACCGGGGTGATTATAGCGCCGGGCTCT-3′
T34S REV	5′-AGAGCCCGGCGCTATAATCACCCCGGTCTGC-3′
S61A FW	5′-CATATCGCGCAAGATATTTATGCCCCATCAGGCGCCAATAAGAGAAAG-3′
S61A REV	5′-CTTTCTCTTATTGGCGCCTGATGGGGCATAAATATCTTGCGCGATATG-3′
S63A FW	5′-GCGCAAGATATTTATTCTCCAGCCGGCGCCAATAAGAGAAAGCCTG-3′
S63A REV	5′-CAGGCTTTCTCTTATTGGCGCCGGCTGGAGTATAAATATCTTGCGC-3′
Q118A FW	5′-GCGGTCAGGAGGTTGCGAATCGGGCGCATC-3′
Q118 REV	5′-GATGCGCCCGATTCGCAACCTCCTGACCGC-3′
H122A FW	5′-CAGGAGGTTCAGAATCGGGCGGCCCGAATAATAGGCGCAGAAAAA-3′
H122A REV	5′-TTTTTCTGCGCCTATTATTCGGGCCGCCCGATTCTGAACCTCCTG-3′
H122Q FW	5′-CAGGAGGTTCAGAATCGGGCGCAGCGAATAATAGGCGCAGAAAAA-3′
H122Q REV	5′-TTTTTCTGCGCCTATTATTCGCTGCGCCCGATTCTGAACCTCCTG-3′

*Primer name indicates the amino acid substitution (FW = forward primer, REV = reverse primer).
†Introduced mutations are underlined.